Carbon-supported $Co_{1.67}Te_2$ nanoparticles as electrocatalysts for oxygen reduction reaction in alkaline electrolyte

Gang Wu,†*[a] Guofeng Cui,[b] Deyu Li,[a] Pei-Kang Shen[b] and Ning Li[a]

Received 23rd February 2009, Accepted 12th June 2009
First published as an Advance Article on the web 14th July 2009
DOI: 10.1039/b903216a

Well-dispersed $Co_{1.67}Te_2$ nanoparticles supported on carbon black have been synthesized *via* a solid-state reaction using Co and Te precursors in an autoclave at elevated temperatures. Their oxygen reduction reaction (ORR) activity and selectivity as a function of heating temperatures in catalyst synthesis were evaluated by rotating disk (RDE) and ring-disk electrodes (RRDE). It was found that the best performing catalyst (CoTe/C-900) was synthesized at a temperature of 900 °C, with regard to the most positive RDE onset (−0.18 V vs Ag/AgCl) and half-wave potentials (−0.35 V vs Ag/AgCl) as well as the lowest peroxide yield (*ca.* 5%) in alkaline solution (0.1 M KOH, pH = 13). Meanwhile, well-defined limiting currents were reached in the mass transfer-controlled potential range at various rotating speeds, attesting to the high density and uniform distribution of ORR active sites on the catalyst. The average electron transfer number of ORR was determined to be 3.5 for the CoTe/C-900 catalyst by using a modified Koutecky–Levich equation, nearly providing a four-electron pathway for the ORR. A transition of the Tafel slope from *ca.* −60 mV/dec to *ca.* −120 mV/dec with overpotential is directly associated with oxide formation and their coverage variation onto catalysts, suggesting a change of the rate-determining step in the ORR mechanism from intermediate-migration to charge-transfer. Extensive physical characterizations including X-ray diffraction (XRD), high-resolution transmission electron microscopy (HR-TEM), and X-ray photoelectron spectroscopy (XPS) were conducted for each CoTe/C sample prepared at various heating temperatures to provide insights into the origins of active sites, and $Co_{1.67}Te_2$ chalcogenide nanoparticles supported on carbon were found to be highly active toward ORR in alkaline electrolytes.

Introduction

Recently, tremendous progress has been made to develop Nafion®-based polymer electrolyte fuel cells (PEFCs), however, there remain significant obstacles in bringing them to market, one of which has been the severe dependence of catalysts on platinum (Pt), an expensive and scarce resource in the earth. Although great efforts have been devoted to exploring low-Pt and even non-precious metal catalysts for PEFCs,[1–3] practical resolution regarding long-term durability[4] and high activity[5] in the strongly acidic nature of Nafion® is still limited. Additionally, poor kinetics for oxygen reduction reaction (ORR) on cathodes in acid environments is another one of the major factors hindering the implementation of low-temperature fuel cells. Alternatively, the use of alkaline media in fuel cell applications presents many advantages, both in electrocatalytic activity and in materials stability, over acidic media.[6,7] Since, according to the Nernst equation, this range shifts by −59 mV for every increase of 1 pH unit, the working potential shifts by nominally −0.83 V as a result of a change from a 1 mol/L H^+ solution of strong acid to a 1 mol/L OH^- solution of strong base.[8] Such a potential shift can dramatically affect the local double-layer structure and the electric field at the electrode-electrolyte interface, leading to changes in adsorption strengths even for neutral species.[9] The decreased extent of spectator anion adsorption in alkaline media means that, in general, most electrocatalytic processes should be more easy in alkaline solutions than in acidic solutions.[10] As a result, especially for ORR, catalysts are indeed performing very favorably in alkaline environments.[6,8,11] While the electrocatalytic advantages of using alkaline media are significant, the improved materials stability afforded by the use of alkaline electrolytes is even more desperately important. A wide variety of materials have exhibited comparable corrosion resistance in alkaline media to that of precious metals, which increases the flexibility to use non-precious materials in fuel cells.[12] Water and ionic transport within the OH^- anion conducting electrolytes also benefit from favorable electroosmotic drag, easily transporting water away and preventing flooding on the cathode, a major issue with PEFCs and direct methanol fuel cells (DMFCs).[13] Meanwhile, this process could mitigate the cross-over problem of methanol, which may offer important advantages in employing alkaline media for DMFCs.[14]

However, alkaline fuel cells (AFCs) have been suffering large performance losses when air is used as oxidant. Specifically, K_2CO_3 precipitated in the air cathode would result in reductions in OH^- concentration, oxygen solubility, electrolyte conductivity and diffusion coefficients, eventually leading to a malfunction of

[a]*Department of Applied Chemistry, Harbin Institute of Technology, Harbin, 150001, China. E-mail: wugang@lanl.gov; Fax: +1-505-6654292; Tel: +1-505-667-3060*
[b]*School of Chemistry and Chemical Engineering, Sun-Yat Sen University, Guangzhou, 510275, China*
† Present address: Los Alamos National Laboratory, MPA-11, Los Alamos, New Mexico 87545, USA.

the gas diffusion electrode, thus causing failure of the entire fuel cell. To combine the advantages of AFCs and PEFCs, a strategy to address this issue is replacing the aqueous alkaline solution with an alkaline polymer electrolyte with cations or anions attached to the polymer chain, leaving no dissociated ions in the liquid phase to form carbonate precipitates. Fortunately, advances in membrane materials and ionomers would make the issue more feasible and allow the development of alkaline-equivalent polymer electrolytes.[6,11,15–18] In particular, the recent breakthrough in quaternary ammonium polysulfones promises a quantum leap in alkaline polymer fuel cell viability.[6] Therefore, prospects for continued development of alkaline electrocatalytic systems based on polymer membrane electrolytes and non-precious metal catalysts will attract more and more interest as an alternative to the more popular proton exchange membrane fuel cells that are prohibitively limited by high cost and low performance.

To data, a wide variety of non-precious catalytic materials have been explored as oxygen cathodes of AFCs in alkaline media. These include nitrogen-doped carbon materials,[19] various transition metals,[20,21] macrocycles (porphyrins[22] and phthalocyanines[23]) and metal oxides[24] (manganese dioxide[25] and various perovskites,[26] pyrochlores,[27] and spinels[28]). Among them, transition metal-based chalcogenide compounds, which are known as a promising class of materials for replacing expensive Pt-based ORR electrocatalysts in alkaline media, have exhibited facile ORR kinetics with minimal peroxide generation, as well as their depolarized character such as insensitivity to methanol and halide ions.[1] Baresel *et al.*[29] once proposed that Co–S and Co–Ni–S systems had higher ORR electrocatalytic activity when compared with other transition metals. They also observed that the minimal energy difference between the oxygen 2p orbital and the highest occupied d orbital of sulfides would be beneficial for better catalytic activity. In the case of cobalt sulfides with various ratios of Co:S, it was found that Co_3S_4 possessed the highest ORR activity and selectivity of direct four-electron oxygen reduction to OH^- in 0.1 M KOH.[30] Susac and Zhu[31–33] further explored the ORR electrocatalytic activity and stability of $Co_{1-x}Se$, FeS_2 and $(Co,Fe)S_2$ thin films (0.4–0.5 μm thickness) prepared by magnetron sputtering onto a glassy-carbon substrate. The possible active sites were attributed to the Co/Fe-deficient crystalline structure with extra chalcogen (Se or S) surrounding. Based on the adsorption bond strengths of the reactants, reaction intermediates, and production for water oxidation and O_2 reduction, the (202) surfaces of Co_9S_8 and Co_9Se_8 ORR catalysts were predicted to be active toward O_2 reduction using adsorption energies calculated with the Vienna ab-initio simulation program (VASP).[34] One structure in the proposed four-electron reduction mechanism is novel: S^{2-} provides an adsorption site for O following O–O bond scission, which, unlike the case of platinum electrodes, takes place prior to the first reduction step.[34] Furthermore, with the aim of increasing the accessible surface area of catalytic materials, and hence to increase their mass activity, chalcogenide nanoparticles such as $CoSe_2$ and Co_3S_4 were successfully synthesized and dispersed onto carbon supports, which were examined as potential ORR catalysts in acidic media.[35] Their performances were found to be greatly dependent on particle size and nanocrystallinity. Here, we have an interest in Te as an element among the transition metal-based chalcogenides. This is because the Te atom has more metallic character than S and Se atoms, which must be a favorable property for electrocatalysts because of good electron conductivity. Another point is that transition metals alloyed with Te have been well known to ameliorate their tolerance of electrochemical oxidation conditions.[36] These unique features of Te seem to be prerequisites to examine it as a non-Pt catalyst for the ORR.

Thus, our attention then focused on evaluating a binary Co–Te system and a new carbon-supported $Co_{1.67}Te_2$ chalcogenide has been synthesized through a solid-state reaction in an autoclave at elevated temperatures, being considering as potential non-precious cathode catalyst for alkaline polymer electrolyte fuel cells (APEFCs). Its ORR catalytic properties were examined using rotating disk/ring electrodes in 0.1 M KOH electrolyte. Kinetic parameters such as Tafel slope were analyzed to address the possible ORR mechanism. Meanwhile, the catalysts were subjected to extensive materials characterization including X-ray diffraction (XRD), high-resolution transmission electron microscopy (HR-TEM), and X-ray photoelectron spectroscopy (XPS).

Experimental

Catalyst preparation

The commercially available Ketjen Black EC 300 J material was adopted as the carbon support for Co–Te catalysts because of its high BET surface area (about 950 m^2/g), large fraction of mesophase and corrosion resistance.[37] To synthesize CoTe/C catalysts, $Co(NO_3)_2 \cdot 6H_2O$ and $TeCl_4$ were used as Co and Te precursors, respectively, due to their good solubility. The basic principles of the synthesis are schematically presented in Fig. 1. Our procedure did not involve any organic solvent in the synthesis and only high purity water was used. The catalyst preparation is briefly described as follows. First, 0.291 g $Co(NO_3)_2 \cdot 6H_2O$ (1 mmol) and 0.269 g $TeCl_4$ (1 mmol) precursors were well dissolved in 300 ml Milli-Q water (18 MΩ cm) with a Co:Te atomic ratio of 1:1. Under vigorous stirring for 1 hour, ultrasonically dispersed carbon black (0.25 g) slurry was added into the above solution maintaining a nominal Co–Te loading of

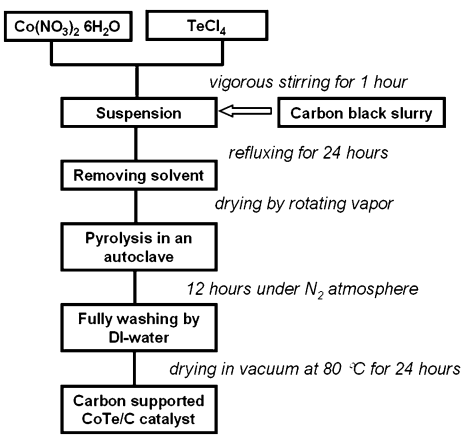

Fig. 1 Schematic representation of the aqueous synthetic procedure used to prepare $Co_{1.67}Te_2$ nanoparticles supported on carbon black.

42.8 wt% on carbon, followed by refluxing for 24 hours. Then, the water was removed by rotating vapor under reduced pressure and the impregnated carbon materials were transferred to an autoclave. The autoclave was sealed and maintained at 300, 600, or 900 °C for 12 hours under nitrogen atmosphere. After cooling naturally to room temperature, the products in the autoclave were collected and washed with distilled water several times to dissolve the unstable species.[38] Final products were obtained by drying under vacuum at 80 °C for 24 hours. In this work, the resulting catalysts from various heating temperatures are labeled as CoTe/C-300, CoTe/C-600 and CoTe/C-900.

Electrochemical characterization

To determine the electrocatalytic activity and selectivity for ORR, rotating ring/disc electrode (RDE and RRDE) measurements for CoTe/C catalysts were performed in a conventional three-electrode cell with 0.1 M KOH (pH = 13) solution using a bipotentiostat (Pine Instruments, Model AFRDE) at room temperature (23 ± 2 °C). Pt wire and potassium chloride saturated silver/silver chloride (Ag/AgCl, KCl-sat., 0.199 V *vs.* SHE) were used as the counter and the reference electrodes, respectively. Catalyst inks were prepared by ultrasonically mixing 10.0 mg catalyst sample and 5 μl polytetrafluoroethylene (PTFE) solution (40 wt%) in 1.0 ml ethanol solution and attached to the glassy carbon rotating disc electrode. In RDE tests, ORR steady-state polarization curves were recorded in oxygen saturated 0.1 M KOH solutions with a potential step of 0.03 V and a period time of 60 s. The disk rotating rates ranged from 300 to 2400 rpm. Meanwhile, RRDE experiments were also carried out in oxygen saturated 0.1 M KOH solution to estimate the percentage of peroxides formed per molecule of reduced oxygen as a function of working potential.[39] Electrochemical stability studies using cyclic voltammetry were also conducted in nitrogen saturated 0.1 M KOH solution at a scan rate of 50 mV/s.

Physical characterization

X-Ray diffraction (XRD) patterns were recorded using a Bruker d8 diffractometer equipped with Cu Kα radiation and a graphite monochromatic operation at 45 kV and 40 mA. The diffraction patterns were scanned at a rate of 1.2 deg/min with a scan step of 0.02 deg. HR-TEM images were taken on a JEOL JEM-2010F with a resolution of 0.102 nm operating at 200 kV to study the morphology of Co–Te particles. High angle annular dark-field STEM was employed to study the Co–Te particle distribution on carbon supports. To determine chemical composition and oxidation states of Co and Te in CoTe/C catalysts, X-ray photoelectron spectroscopy (XPS) analysis was performed on an ESCA 210 and a MICROLAB 310D spectrometer using Mg Kα ($h\nu = 1253.6$ eV) irradiation as the photon source with a primary tension of 12 kV and an emission current of 20 mA.

Results and discussion

ORR performance

ORR steady-state activity and four-electron selectivity data for each CoTe/C catalyst in 0.1 M KOH at a rotating rate of 1200 rpm are shown in Fig. 2. Among various heating temperatures, the catalyst synthesized from 900 °C (CoTe/C-900) presents the most positive RDE onset (−0.18 V vs Ag/AgCl) and half-wave potentials (−0.35 V vs Ag/AgCl) shown in Fig. 2a, suggesting the highest ORR catalytic activity. The relatively positive half-wave potentials also mean that the number of robust active sites is increasing with the heating temperature, being favorable to catalyze oxygen reduction. However, according to Ahmadpour and Do, further increasing the pyrolysis temperature for porous carbon black materials can induce shrinkage of the carbon structure,[40] resulting in a lower porosity and a poor distribution of loaded particles. Thus, at this point, the tentatively optimized temperature employed in this work is 900 °C. A charge-transfer kinetics control potential range, followed by a well-defined current plateau controlled by mass transfer was observed for the CoTe/C-900 catalyst, attesting to the high density and uniform distribution of ORR active sites on the catalyst. On the other hand, in RRDE tests, the correlations between the generated HO_2^- and the potential for each CoTe/C catalyst are shown in Fig. 2b. It can be found that generation of HO_2^- during oxygen reduction was restricted on the catalyst obtained at higher heating temperatures. In particular, the HO_2^- yield declined from 35% for CoTe/C-300 to 15% for CoTe/C-600, and finally to 5% on CoTe/C-900 catalyst at −0.58 V vs Ag/AgCl. Generally, the carbon materials are also able to electroreduce oxygen to

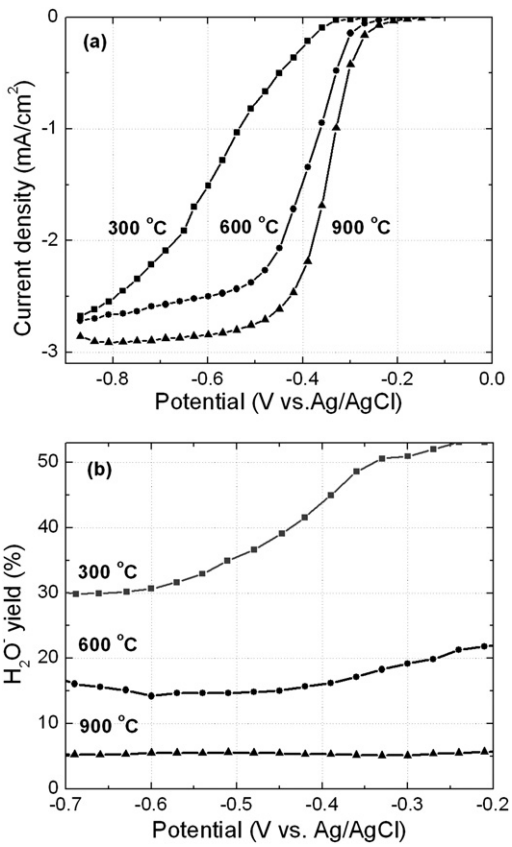

Fig. 2 Steady-state measurements of ORR catalytic activity (a) and selectivity (b) for each CoTe/C catalyst in 0.1 M KOH solution saturated with oxygen at a rotating speed of 1200 rpm and room temperature. Currents are normalized to the geometric surface area. For clarity, only the positive sweeps are shown.

peroxide mainly through a two-electron route.[41] Therefore, the higher yield of HO_2^- for the CoTe/C-300 catalyst may be partially attributed to the adsorption of O_2 onto the weak active sites provided by the carbon supports. The remarkable decrease in HO_2^- yield resulting from pyrolysis at higher temperatures is likely due to two reasons: one is that new active sites with better catalytic ability to effectively adsorb and dissociate O_2 were produced; the other is that the thermal treatment simultaneously increases the number of suitable active sites and decreases the number of weak sites which form HO_2^-.

Fig. 3 shows ORR polarization curves for the best performing CoTe/C-900 catalyst subjected to different electrochemically cycling. It was found that the half-wave potential, initially about −0.35 V vs. Ag/AgCl, insignificantly decreases to −0.37 V after 1000 electrochemical cycles between −0.8 V and −0.4 V vs Ag/AgCl in nitrogen-saturated 0.1 M KOH solution. However, a larger decline in half-wave potential to −0.45 V vs Ag/AgCl was observed after 1000 cycles between −0.8 V and 0 V vs Ag/AgCl. In both cycling experiments, it can be seen that the ORR onset potentials were nearly identical, suggesting that, regardless of the upper-potentials employed for the electrochemical cyclings, the nature of the active sites remains unchanged. Thus, the performance loss indicated by the negative shifts in the half-wave potentials is due to a pronounced loss of active sites, especially the larger degradation in cycling with higher upper-potential. Generally, it is recognized that corrosion of the carbon support has a major impact on catalyst performance degradation. Severe damage to the carbon black structure has been observed after a PEFC power-cycled and start-up/shut-down operation representative of automotive applications. In-line direct gas mass spectroscopy analysis also obviously detected intermittent peaks of carbon dioxide emission from the cathode, indicating that carbon corrosion occurs during the load cycle in the PEFC.[42] As a result, oxygen-containing groups (*e.g.*, carboxyl, carbonyl, hydroxyl, and phenol) are formed on the degraded carbon support surface. The presence of oxygen-containing groups can both decrease the conductivity of catalysts and weaken the interaction between support and nanoparticles which results in an accelerated sintering or detachment for these catalytic metal nanoparticles.[43] Thus, the degradation in RDE activity is primarily associated with the oxidation of carbon supports and subsequent agglomeration of Co–Te particles during electrochemical cycling. Meanwhile, another possible explanation for the reduction in the number of active sites would be the dissolution of the Co–Te or one of the alloy components in the alkaline electrolyte, which is still under study using ICP-MS analysis.

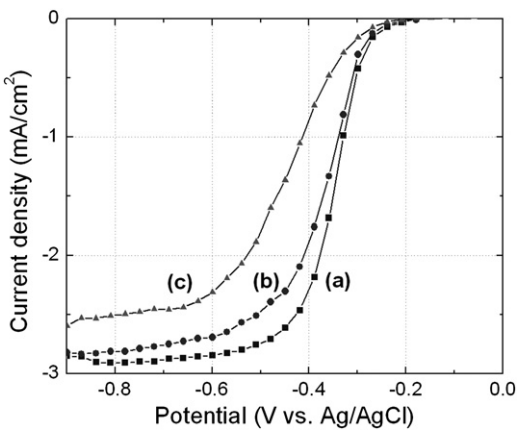

Fig. 3 Steady-state measurements of CoTe/C-900 catalyst recorded in the oxygen-saturated 0.1 M KOH solution at a rotating speed of 1200 rpm subjected to different electrochemically cycling conditionings: (a) as-prepared catalyst; (b) after 1000 electrochemical cycles between −0.8 and −0.4 V vs Ag/AgCl; (c) after 1000 electrochemical cycles between −0.8 and 0 V vs Ag/AgCl. Scanning rate is 50 mV/s and electrolyte for cycling is N_2-purged 0.1 M KOH solution.

ORR kinetic analysis

The electrocatalytic activity for the best performing CoTe/C-900 catalyst was quantitatively examined as a function of rotating speed ranging from 300 to 2400 rpm, as shown in Fig. 4a. The well-defined limiting current at each rotating speed suggests the charge transfer rates during ORR are much faster comparing with the mass transportation rates. Koutecky-Levich plots as a function of ORR working potentials for the CoTe/C-900 catalyst are shown in Fig. 4b. These lines overlapping or remaining parallel to each other indicate that the number of electrons transferred in ORR barely changes within the potential region of the limiting-current. We compared the slopes of these

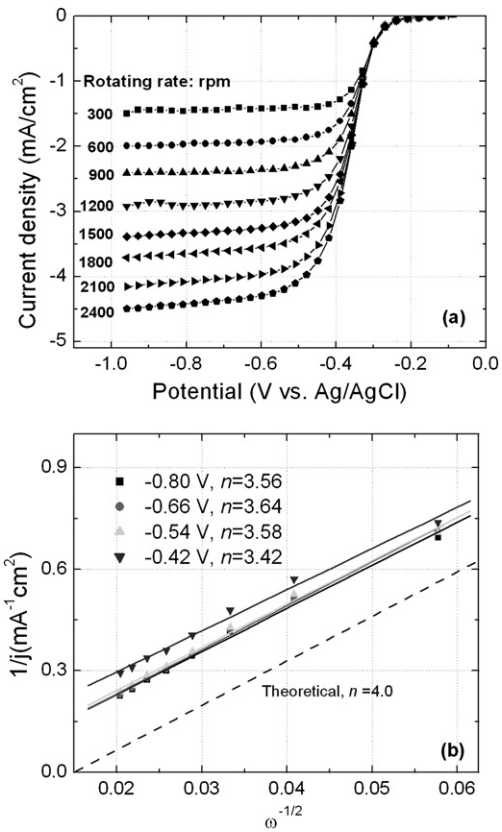

Fig. 4 (a) RDE steady-state polarization curves for the ORR on the CoTe/C-900 catalyst in oxygen-saturated 0.1 M KOH solution at various rotating rates, as indicated next to the curves (in rpm); (b) Koutecky-Levich plots for the ORR on the CoTe/C-900 catalyst at different electrode potentials. Dashed line shows the theoretical slope for $n = 4$; potentials refer to the Ag/AgCl reference electrode.

plots with the theoretically calculated value for four-electron O_2 reduction using the modified Koutecky-Levich equation for a film-coated electrode.[44,45] The overall measured current (j) is related to the kinetic current (j_k), the boundary-layer diffusion-limiting current (j_d), and the film diffusion-limiting current (j_f). The diffusion-limiting current can be represented by equation (1):

$$j_d = 0.2nFD_o^{2/3}C_o\nu^{-1/6}\omega^{1/2} \quad (1)$$

F is the Faraday constant, D_o is the diffusion coefficient of O_2 (1.9×10^{-5} cm^2/s), ω is the electrode rotation rate in units of rpm, ν is the kinematic viscosity of water (0.01 cm^2/s), and C_o is the concentration of O_2 in dilute aqueous solution (1.1×10^{-6} mol/cm^3). The value of j_f is controlled by O_2 diffusion in the catalyst layer defined as a function of the catalyst layer thickness, L, according to:

$$j_f = (nFC_fD_f)L^{-1} \quad (2)$$

where D_f and C_f represent the diffusion coefficient and the solubility of oxygen in the catalyst layer, respectively, independent of rotating speed and other factors. Also, the kinetic current, j_k is exclusively dependent on the catalyst itself. Therefore, the relationship between the measured current density and the rotating speed can be described as follows:

$$\frac{1}{j} = \frac{1}{j_k} + \frac{1}{j_f} + \frac{1}{j_d} = \frac{1}{j_k} + \frac{L}{nFC_fD_f} + \frac{1}{B\omega^{1/2}} = A + \frac{1}{B\omega^{1/2}} \quad (3)$$

A is a constant which represents the nature of the catalyst site (j_k) and the structure of the catalyst layer (j_f), while B typically is the Levich constant that can be obtained from the slopes of the Koutecky-Levich plots. Using the appropriate numerical values,[46] the relationship between the B value and the number of electrons transferred n during the ORR can be further reasonably simplified as

$$B = 0.2nFD_o^{2/3}C_o\nu^{-1/6} = 3.5 \times 10^{-5}n \quad (4)$$

Thus, by calculating the slopes of the Koutecky-Levich plots in Fig. 4b, an n value of 3.42–3.64 (average: 3.5) was obtained for the CoTe/C-900 catalyst in the potential range from −0.80 V to −0.42 V vs Ag/AgCl. It indicates that in alkaline aqueous media, the catalyst is able to electrocatalytically reduce O_2 to OH^- mostly through a direct four-electron or a two + two route in the regions controlled by mass diffusion and mixed kinetic-diffusion.

Tafel slopes (b) were obtained to further evaluate the ORR kinetic character of CoTe/C catalysts in alkaline media. Kinetic current densities extracted from the steady-state polarization according to the Koutecky-Levich equation were used to plot these Tafel plots. The linear fitted Tafel slopes for each CoTe/C catalyst at high and low potential ranges are shown in Fig. 5a and b, respectively. In the case of the CoTe/C-300 sample showing poor ORR performance, Tafel slopes of −123 mV/dec at high potential and −42 mV/dec at low potential range were obtained. Unlike the CoTe/C-300 sample, the Tafel slopes of CoTe/C-600 and CoTe/C-900 are close to −59 mV/dec in the high potential range (>−0.28 V vs Ag/AgCl), while at low potential values around −120 mV/dec were observed. The similar Tafel slopes for

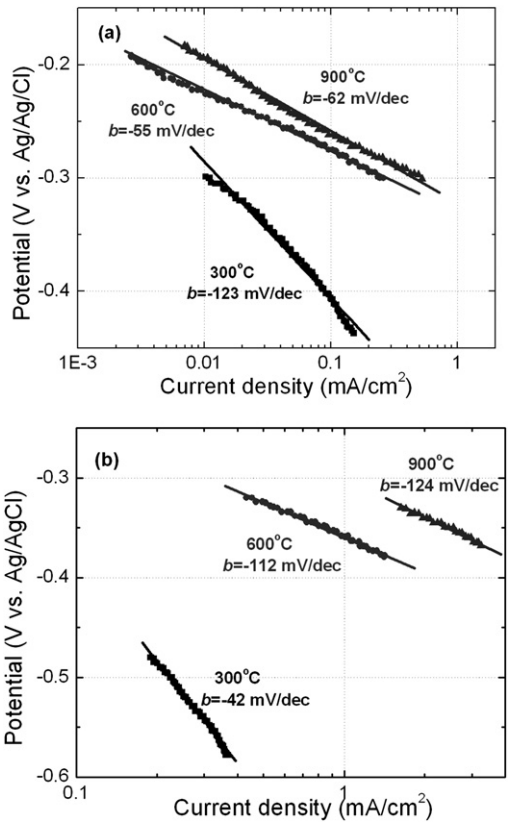

Fig. 5 ORR Tafel plots at high potentials (a) and low potentials (b) over each CoTe/C catalyst synthesized at various heating temperatures.

CoTe/C-600 and CoTe/C-900 samples suggest that, in both cases, ORR should occur on identical active sites through similar mechanisms. In contrast, the formation of new active sites associated with Co–Te species at elevated heating temperatures such as 900 °C probably accounts for the significant difference in Tafel slope between the best performing CoTe/C-900 and the worst CoTe/C-300. In general, oxygen reduction in aqueous alkaline media is a complicated electrocatalytic reaction. Many species have been proposed as intermediates in this multi-step reaction, including O, OH, O_2^-, and HO_2^-, leading to a great number of possible mechanisms.[47] Somewhat similar Tafel slopes once were observed during oxygen reduction on Pt electrodes in alkaline media by Damjanovic and coworkers.[48] At high potentials, the Tafel slope was found to be 60 mV/dec, while the pH dependence (at constant current) was −30 mV per pH unit. At low potentials, the measured Tafel slope was 120 mV/dec while the pH dependence was 0 mV per pH unit. Theoretically, a Tafel slope of 118 mV/dec is due to the rate-determining step associated with the first electron transfer leading to roughly Langmuirian adsorption, while a Tafel slope around 59 mV/dec had been ascribed to the coverage of adsorbed oxygen, with a Temkin adsorption of O at higher coverage of oxide or adsorbed oxygen intermediates, leading to a coverage-dependent activation barrier for electrochemical reactions.[48,49] Moreover, such behavior of the Tafel line is quite analogous to that reported for Co based oxide electrodes for the oxygen evolution reaction (OER) in alkaline media.[50] Thus, this transition of the ORR Tafel slope for CoTe/C catalysts is probably related to the formation of cobalt oxide and

its coverage, indicative of an ORR mechanism transition from intermediate-migration control to charge-transfer control with increasing overpotential. In charge control potential ranges, Damjanovic also suggested, along with the observed first-order dependence on O_2 partial pressure, a rate-limiting first electron transfer to adsorbed O_2 to form superoxide (equation 5), possibly involving a concurrent reaction with water (equation 6).[48]

$$Me–O_2 + e^- \rightarrow Me–O_2^- \quad (5)$$

$$Me–O_2 + H_2O + e^- \rightarrow Me–HO_2 + OH^- \quad (6)$$

Recently, IR spectra[51] reveal the presence of adsorbed O_2^- during the ORR on Pt at pH = 11, indicating that equation 5 is more likely to be the first step than equation 6. Computational investigations have also supported the Damjanovic mechanism, with the energy barrier for protonation of O_2 found to be lower than that for the O–O bond.

To understand the likely active sites responsible for the high ORR activity in CoTe/C catalysts, physical characterization for each catalyst synthesized at various heating temperatures was conducted using XRD, HR-TEM, and XPS techniques.

XRD analysis

XRD was used to determine the crystal structure for each CoTe/C catalyst and the patterns obtained are compared in Fig. 6. Beside the carbon (002) peaks at about 2θ = 25.5°, only the diffraction peaks related to the metallic Co phase (2θ = 44.3°, 51.3° and 75.6°) were detected in the CoTe/C-300 catalyst. However, with pyrolysis temperature increasing, especially, in the case of CoTe/C-900 catalysts, dominant presence of diffraction peaks (2θ = 31.4°, 33.3°, 43.0°, 46.7°, 57.3°, 58.3°, 65.3°, 70.0°, 76.9 and 77.8°) assigned to the $Co_{1.67}Te_2$ phase was observed.[52] It was known that the chalcogens can form chalcogenides with transition metals (*e.g.* Fe, Co and Ni) having a wide variety of stoichiometry.[53] The Co–Te systems with various compositions have also been investigated with respect to the crystallographic, thermal, electrical and magnetic properties.[54–56] The cobalt telluride with the composition of $Co_{1.67}Te_2$ that was successfully synthesized through a solid-state reaction in this work belongs to the P3-M1 space group and the stable trigonal CdI_2-type structure with a polymeric network containing multiple Te–Te bonds.[54] It was also confirmed as a kind of intermetallic compound using experimental valence band spectra (UPS),[54] showing typical metallic conductivity. As the electrochemical measurements indicated, the high ORR activity of the carbon supported CoTe catalyst should be attributed to the formation of $Co_{1.67}Te_2$, providing a new kind of active site for oxygen adsorption and dissociation in alkaline media. It is worth noting that the relative intensities of peaks assigned to $Co_{1.67}Te_2$ in the CoTe/C-600 sample are apparently lower than those in CoTe/C-900. This is probably the reason why CoTe/C-900 exhibited better ORR performance than CoTe/C-600, suggesting that the formation of active $Co_{1.67}Te_2$ species benefits from higher thermal temperatures.

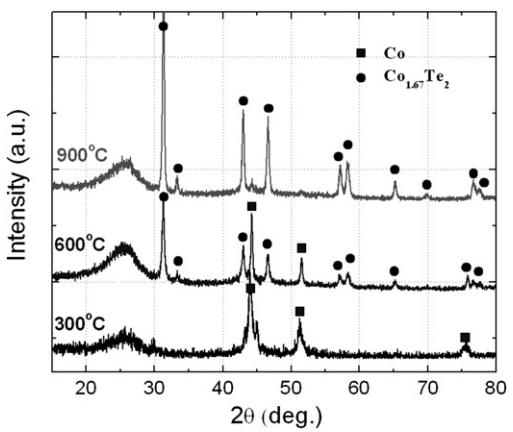

Fig. 6 XRD patterns for each CoTe/C catalyst synthesized at various heating temperatures.

HR-TEM and STEM images

To investigate the effect of heating temperature on the surface morphology and structure of carbon supported $Co_{1.67}Te_2$ catalysts, the representative HR-TEM images for each CoTe/C catalyst synthesized at various heating temperatures are compared in Fig. 7. Before pyrolysis (Fig. 7a), there are very few apparent solid particles on the carbon support, suggesting the cobalt and tellurium precursors fully adsorb onto porous carbon black in the forms of ions or amorphism. Combined with the XRD analysis, scattered particles in the CoTe/C-300 sample (Fig. 7b) can be mainly assigned to metallic Co species when the heating temperature is 300 °C. Although $Co_{1.67}Te_2$ chalcogenide particles appear when the heating temperature is as high as 600 °C (Fig. 7c), much denser nanoparticle morphology and better distribution were observed at 900 °C (Fig. 7d), which means heat treatment at higher temperature is favorable for the generation of $Co_{1.67}Te_2$ particles. Like the Pt/C catalyst, the higher utilization of the active materials can contribute more sites for oxygen reduction, thereby showing higher mass activity. This is probably the reason that the ORR half-wave potential for CoTe/C-900 is

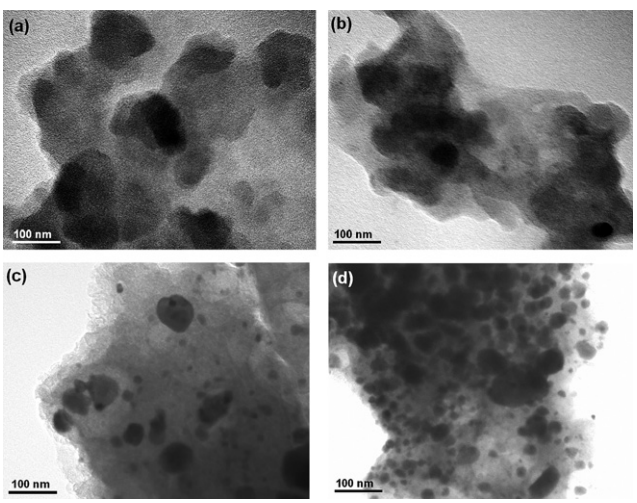

Fig. 7 Representative HR-TEM images for each CoTe/C catalyst synthesized at various heating temperatures (a) un-pyrolyzed; (b) 300 °C; (c) 600 °C; (d) 900 °C.

60 mV more positive than that for CoTe/C-600 catalysts. Although generally high temperature favors particle agglomeration, the particle size observed for CoTe/C-900 is smaller than that of the CoTe/C-600 sample. It should be recognized that the formation of nanoparticle has two distinct stages. The first stage is the formation of nuclei of the new phase. The nuclei then grow into bigger particles with time. Usually, the increase of nanoparticle size with temperature is attributed to the fact that the number of nuclei on carbon is insufficient. In the solid-state reaction employed in this work, to overcome the activation energy and form new $Co_{1.67}Te_2$ seeds, increasing the temperature to 900 °C for example only resulted in an increase in the number of $Co_{1.67}Te_2$ nuclei, and not an obvious growth in the size of the particles, thereby resulting in a well-dispersed particle morphology.

A temperature of 900 °C was tentatively optimized for the carbon supported $Co_{1.67}Te_2$ catalyst synthesis in this work. Thus, further optimization of the $Co_{1.67}Te_2$ morphology and distribution by tuning the synthesis chemistry and using more suitable carbon supports would constantly keep the ORR catalytic activity moving forward. Furthermore, the STEM image of a carbon supported CoTe/C-900 catalyst is shown in Fig. 8a. Excluding some extra large aggregates, the particle size distribution (PSD) based on 100 particles at random determined from the image is also shown in Fig. 8b, presenting a mean particle size of 30 ± 15.0 nm.

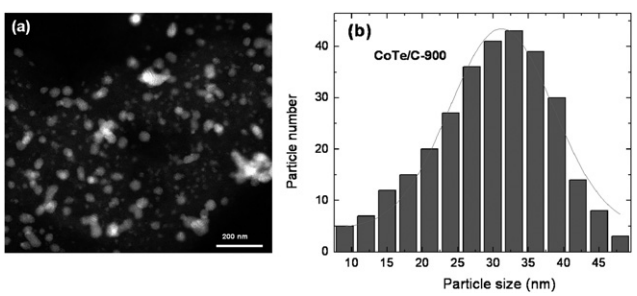

Fig. 8 Representative STEM image of the CoTe/C-900 catalyst (a) and its particle size distribution (PSD) (b).

XPS analysis

Generally, the catalytic performance of electrocatalysts is very sensitive to their surface or subsurface composition and oxidation state. X-Ray photoelectron spectroscopy (XPS) seems to be the most successful method to study the solid electrocatalyst materials. Here, the effect of heating temperature on surface states of CoTe/C catalysts was studied by XPS. Co 2p and Te 3d core level spectra for each CoTe/C sample are shown in Fig. 9a and b, respectively.

With pyrolysis temperature increasing, the Co 2p spectra gradually split from a broad peak to two dominant peaks. In particular, as for un-pyrolyzed sample, through Gaussian-Lorentzian fitting, a broad peak around 779.5–782.5 eV associated with various Co(II) and Co(III) species[57] reveals that no metallic Co species were formed before pyrolysis. When the sample was treated at 300 °C, although peaks assigned to cobalt oxides still dominate, metallic Co species appear to be emerging at 778.2 eV.

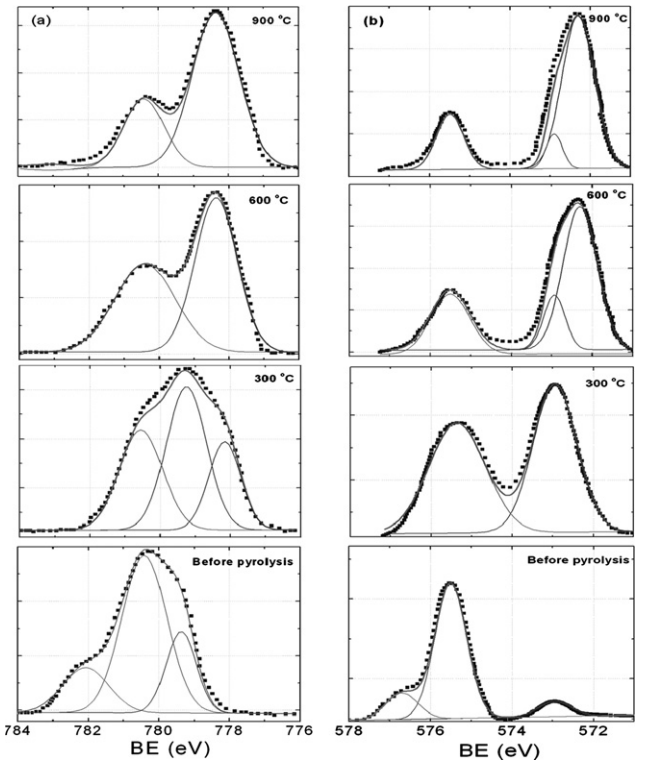

Fig. 9 Co 2p (a) and Te 3d (b) XPS spectra for each CoTe/C catalyst synthesized at various heating temperatures.

However, in the case of the sample treated at 600 °C, a peak located at 778.5 eV is apparently manifested with a higher binding energy than that of the metallic Co species at 778.2 eV observed at 300 °C. Furthermore, when the heating temperature was further increased to 900 °C, the peak at 778.5 eV becomes pronounced. In general, the evaluated binding energies for the Co $2p_{3/2}$ level are averaged at 778.2 eV for elemental Co according to the NIST XPS database. With the addition of Te, the electron density located on the Co centres would be reduced and the Co–Co distance becomes shorter.[54] As a result, the binding energy of the cobalt tellurides would shift to higher energy when compared with that of elemental Co. Thus, the peak located at 778.5 eV can be rotationally assumed as $Co_{1.67}Te_2$, in very good agreement with what is expected based on XRD and HR-TEM analysis. Unlike other Co chalcogenides such as Co_9S_8 (778.5 eV), $CoSe_2$ (778.3 eV)[58] and CoSe (778.7 eV)[59] which also exhibited higher binding energy, $Co_{1.67}Te_2$ is an intermetallic compound and more like a metal. Furthermore, from the viewpoint of qualitative analysis, the increasing intensity of Co–Te bonds with heating temperature in catalyst synthesis provides direct evidence to understand that better ORR activity is correlated to higher content of $Co_{1.67}Te_2$.

Te 3d spectra for each CoTe/C catalyst treated at various temperatures are shown in Fig. 9b. Before pyrolysis, except for a small peak at low binding energy belonging to metallic Te, there are two obvious peaks located at around 575.5 eV and 576.7 eV that can be assigned to Te^{4+} and Te^{6+}, respectively. It was found the pyrolysis leads to the formation of another broad peak located at low binding energy generally associated with metallic Te species, which can be further split into a major peak

at 572.3 eV and a small peak at 572.9 eV. As the oxidation number for Te is less than −1 in $CoTe_x$ intermetallic compounds,[54] the peak located at 572.3 eV can be assigned to $Co_{1.67}Te_2$, leading to a shift of 0.6 eV relative to elemental Te (*ca.* 572.9 eV[54]) based on a linear relationship between the chemical shift of the Te $3d_{5/2}$ core level and the oxidation number, about 0.6 eV per oxidation number. Compared with the binding energies reported for $IrTe_2$ (573.0 eV) or Ir_3Te_8 (573.5 eV)[60] and $NbTe_4$ (572.8 eV),[61] the value obtained for $Co_{1.67}Te_2$ is lower, but is very close to those of ZrSiTe (572.5 eV),[62] CdTe (572.47 eV)[63] and $NiTe_2$ (572.3 eV).[64] It can be also seen that, with an increase in heat treatment temperature, the Te–Co peak at 572.3 eV gradually increases, while the Te–O peak at 575.5 eV becomes less dominant, which means that oxide was reduced and new Te–Co bonds were formed at higher temperatures. This correlation between temperature of pyrolysis and formation of $Co_{1.67}Te_2$ species is in good agreement with XRD and HR-TEM analyses.

Conclusion

In summary, well-dispersed $Co_{1.67}Te_2$ nanoparticles supported on carbon black were successfully synthesized using Co and Te precursors at elevated temperatures in an autoclave, confirmed by XRD, HR-TEM and XPS analyses. The content and particle distribution on supports were found to be strongly depended on the heating temperature. The tentatively optimum temperature to effectively synthesize $Co_{1.67}Te_2$ intermetallic compound is as high as 900 °C at this point, providing more active sites and exhibiting the best ORR performance. As a new non-precious metal cathode catalyst for potential fuel cell applications, the carbon-supported $Co_{1.67}Te_2$ chalcogenide nanoparticles demonstrated promising activity and stability for oxygen reduction in alkaline media. The Koutecky-Levich equation analysis further indicated that oxygen can be reduced to OH^- with high selectivity through a four-electron pathway. A transition of the Tafel slope from −60 mV/dec to −120 mV/dec with overpotential for the $Co_{1.67}Te_2$ catalyst is indicative of an ORR mechanism change from intermediate (O, OH, O_2^-, or HO^{2-}) migration control to first electron transfer control, relating to the variation of oxide coverage on the catalyst. As a kind of intermetallic compound, $Co_{1.67}Te_2$ contains a polymeric network with multiple Te–Te bonds[54] that could be beneficial for oxygen adsorption and subsequent dissociation. But the mechanisms involved remain unknown, including the configuration of active sites, the roles of Co and Te, and whether the electron transfer primarily occurs through bond or through-space tunneling.[33] As a matter of fact, increasing Te content in $CoTe_x$ would decrease the Co–Te distance and reduce the 3d electron density on the Co centre;[54] further optimization of the Co:Te ratio as well as the surface morphology can be expected to generate highly efficient non-precious metal Co–Te electrocatalysts for advanced alkaline fuel cells (AFCs) and alkaline polymer electrolyte fuel cells (APEFCs).

Acknowledgements

The authors acknowledge the financial support of this work from the Postdoctoral Science Foundation (2004035300), the National Natural Science Foundation of China (50801070), and the Plant Nursery Projects of Guangdong Province.

References

1 Y. J. Feng and N. Alonso-Vante, *Phys. Status Solidi B*, 2008, **245**, 1792.
2 H. S. Liu, Z. Shi, J. L. Zhang, L. Zhang and J. J. Zhang, *J. Mater. Chem.*, 2009, **19**, 468.
3 A. Sarkar, A. V. Murugan and A. Manthiram, *J. Mater. Chem.*, 2009, **19**, 159.
4 Y. Shao, J. Liu, Y. Wang and Y. Lin, *J. Mater. Chem.*, 2009, **19**, 46.
5 H. A. Gasteiger, S. S. Kocha, B. Sompalli and F. T. Wagner, *Appl. Catal. B-Environ.*, 2005, **56**, 9.
6 S. F. Lu, J. Pan, A. B. Huang, L. Zhuang and J. T. Lu, *P. Natl. Acad. Sci. USA*, 2008, **105**, 20611.
7 H. Meng, M. Wu, X. X. Hu, M. Nie, Z. D. Wei and P. K. Shen, *Fuel Cells*, 2006, **6**, 447.
8 J. S. Spendelow and A. Wieckowski, *Phys. Chem. Chem. Phys.*, 2007, **9**, 2654.
9 S. A. Wasileski, M. T. M. Koper and M. J. Weaver, *J. Chem. Phys.*, 2001, **115**, 8193.
10 N. M. Markovic and P. N. Ross, *Surf. Sci. Rep.*, 2002, **45**, 121.
11 H. W. Zhang and Z. T. Zhou, *J. Appl. Poly. Sci.*, 2008, **110**, 1756.
12 J. L. Fernandez, D. A. Walsh and A. J. Bard, *J. Am. Chem. Soc.*, 2005, **127**, 357.
13 K. Matsuoka, Y. Iriyama, T. Abe, M. Matsuoka and Z. Ogumi, *J. Power Sources*, 2005, **150**, 27.
14 K. Scott, E. Yu, G. Vlachogiannopoulos, M. Shivare and N. Duteanu, *J. Power Sources*, 2008, **175**, 452.
15 H. Hou, G. Sun, R. He, B. Sun, W. Jin, H. Liu and Q. Xin, *Int. J. Hydrogen Energ*, 2008, **33**, 7172.
16 D. Stoica, F. Alloin, S. Marais, D. Langevin, C. Chappey and P. Judeinstein, *J. Phys. Chem. B*, 2008, **112**, 12338.
17 A. E. S. leightholme, J. R. Varcoe and A. R. Kucernak, *Electrochem. Commun.*, 2008, **10**, 151.
18 G. G. Wang, Y. M. Weng, D. Chu, D. Xie and R. R. Chen, *J. Membrane Sci.*, 2009, **326**, 4.
19 K. Gong, F. Du, Z. Xia, M. Durstock and L. Dai, *Science*, 2009, **323**, 760.
20 T. J. Schmidt, V. Stamenkovic, M. Arenz, N. M. Markovic and P. N. Ross, *Electrochim. Acta*, 2002, **47**, 3765.
21 J. W. Kim and A. A. Gewirth, *J. Phys. Chem. B*, 2006, **110**, 2565.
22 S. L. Gojkovic, S. Gupta and R. F. Savinell, *J. Electroanal. Chem.*, 1999, **462**, 63.
23 C. J. Song, L. Zhang and J. J. Zhang, *J. Electroanal. Chem.*, 2006, **587**, 293.
24 L. Jorissen, *J. Power Sources*, 2006, **155**, 23.
25 L. Q. Mao, T. Sotomura, K. Nakatsu, N. Koshiba, D. Zhang and T. Ohsaka, *J. Electrochem. Soc.*, 2002, **149**, A504.
26 A. Hammouche, A. Kahoul, D. U. Sauer and R. W. D. Doncker, *J. Power Sources*, 2006, **153**, 239.
27 H. S. Horowitz, J. M. Longo and H. H. Horowitz, *J. Electrochem.Soc.*, 1983, **130**, 1851.
28 N. Heller-Ling, M. Prestat, J. L. Gautier, J. F. Koenig, G. Poillerat and P. Chartier, *Electrochim. Acta*, 1997, **42**, 197.
29 D. Baresel, W. Sarholz, P. Scharner and J. Schmitz, *Ber. Bunsen-Ges.*, 1974, **78**, 608.
30 T. Osaka, Y. Iwase, H. Kitayama and T. Ichino, *Bull. chem. Soc. Jpn*, 1983, **56**, 2106.
31 D. Susac, A. Sode, L. Zhu, P. C. Wong, M. Teo, D. Bizzotto, K. A. R. Mitchell, R. R. Parsons and S. A. Campbell, *J. Phys. Chem. B*, 2006, **110**, 10762.
32 D. Susac, L. Zhu, M. Teo, A. Sode, K. C. Wong, P. C. Wong, R. R. Parsons, D. Bizzotto, K. A. R. Mitchell and S. A. Campbell, *J. Phys. Chem. C*, 2007, **111**, 18715.
33 L. Zhu, D. Susac, M. Tea, K. C. Wong, P. C. Wong, R. R. Parsons, D. Bizzotto, K. A. R. Mitchell and S. A. Campbell, *J. Catal.*, 2008, **258**, 235.
34 R. A. Sidik and A. B. Anderson, *J. Phys. Chem. B*, 2006, **110**, 936.
35 Y. J. Feng, T. He and N. Alonso-Vante, *Chem. Mater.*, 2008, **20**, 26.
36 Y. Hara, N. Minami and H. Itagaki, *Appl. Catal. A: Gen.*, 2008, **340**, 59.
37 G. Wu, D. Li, C. Dai, D. Wang and N. Li, *Langmuir*, 2008, **24**, 3566.

38 G. Wu, R. Swaidan, D. Li and N. Li, *Electrochim. Acta*, 2008, **53**, 7622.
39 U. A. Paulus, T. J. Schmidt, H. A. Gasteiger and R. I. Behm, *J. Electroanal. Chem.*, 2001, **495**, 134.
40 A. Ahmadpour and D. D. Do, *Carbon*, 1996, **34**, 471.
41 S. Maldonado and K. J. Stevenson, *J. Phys. Chem. B*, 2005, **109**, 4707.
42 A. A. Franco and M. Gerard, *J. Electrochem. Soc.*, 2008, **155**, B367.
43 Y. Shao, J. Wang, R. Kou, M. Engelhard, J. Liu, Y. Wang and Y. Lin, *Electrochimica Acta*, 2009, **54**, 3109.
44 D. R. Lawson, L. D. Whiteley, C. R. Martin, M. N. Szentimay and J. I. Song, *J. Electrochem. Soc.*, 1988, **135**, 2247.
45 P. Wang, Z. Ma, Z. Zhao and L. Jia, *J. Electroanal. Chem.*, 2007, **611**, 87.
46 H. C. Ye and R. M. Crooks, *J. Am. Chem. Soc.*, 2007, **129**, 3627.
47 J. L. Valdes and H. Y. Cheh, *J. Electrochem. Soc.*, 1985, **132**, 2635.
48 D. B. Sepa, M. V. Vojnovic and A. Damjanovic, *Electrochim. Acta*, 1980, **25**, 1491.
49 G. Wu, L. Li and B. Q. Xu, *Electrochim. Acta*, 2004, **50**, 1.
50 G. Wu, N. Li, D. R. Zhou, K. Mitsuo and B. Q. Xu, *J. Solid State Chem.*, 2004, **177**, 3682.
51 M. H. Shao, P. Liu and R. R. Adzic, *J. Am. Chem. Soc.*, 2006, **128**, 7408.
52 H. Haraldsen, F. Groenvold and T. Hurlen, *Zeitschrift fuer Anorganische und Allgemeine Chemie*, 1956, **283**, 143.
53 J. Neuhausen, V. K. Evstaf'iev, T. Block, E. W. Finckh, W. Tremel, L. Augustin, H. Fuchs, D. Voss, P. Kruger and A. Mazur, *J. Pollmann. Chem. Mater.*, 1998, **10**, 3870.
54 M. Muhler, W. Bensch and M. Schur, *J. Phys-Condensed Mater.*, 1998, **10**, 2947.
55 P. Terzieff, *Solid State Commun.*, 1984, **50**, 151.
56 H. Binczycka, S. S. Hafner, G. Moh and J. Stanek, *Phys. Lett.*, 1990, **467**, 145A.
57 N. Moslemzadeh, G. Beamson, P. Tsakiropoulos, J. F. Watts, S. R. Haines and P. Weightman, *J. Electron. Spectros. Relat. Phenom.*, 2006, **152**, 129.
58 H. van der Heide, R. Hemmel, C. F. van Bruggen and C. Haas, *J. Solid State Chem.*, 1980, **33**, 17.
59 A. B. Mandale, S. Badrinarayarian, S. K. Date and A. P. B. Sinha, *J. Electron. Spectrosc. Relat. Phenom.*, 1984, **33**, 61.
60 S. Jobic, R. Brec and J. Rouxel, *J. Solid State Chem.*, 1992, **96**, 169.
61 M. K. Bahl, *J. Phys. Chem. Solids*, 1975, **36**, 485.
62 M. Muhler, W. Bensch, O. Helmer, M. Knecht and H. Ebert, *J. Phys. Chem. B*, 1994, **99**, 3326.
63 H. S. White, A. J. Ricco and M. S. Wrighton, *J. Phys. Chem. B*, 1983, **87**, 5140.
64 W. Bensch, W. Heid, M. Muhler, S. Jobic, R. Brec and J. Rouxel, *J. Solid State Chem.*, 1996, **121**, 87.